Published in final edited form as:
Clin Cancer Res. 2014 July 1; 20(13): 3521–3530. doi:10.1158/1078-0432.CCR-14-0395.

Old drug new use - Amoxapine and its metabolites as potent bacterial β-glucuronidase inhibitors for alleviating cancer drug toxicity

Ren Kong[1], **Timothy Liu**[1], **Xiaoping Zhu**[1], **Syed Ahmad**[2], **Alfred L. Williams**[2], **Alexandria T Phan**[3], **Hong Zhao**[1,*], **John E. Scott**[2,*], **Li-An Yeh**[2], and **Stephen TC Wong**[1,3]

[1]Department of Systems Medicine and Bioengineering, Houston Methodist Research Institute, Weill Cornell Medical College, Houston, TX 77030

[2]Biomanufacturing Research Institute and Technology Enterprise, North Carolina Central University, Durham, NC 27707

[3]Methodist Cancer Center, Houston Methodist Hospital, Houston, TX 77030

Abstract

Purpose—Irinotecan (CPT-11) induced diarrhea occurs frequently in cancer patients and limits its usage. Bacteria β-glucuronidase (GUS) enzymes in intestines convert the non-toxic metabolite of CPT-11, SN-38G, to toxic SN-38, and finally lead to damage of intestinal epithelial cells and diarrhea. We previously reported amoxapine as potent GUS inhibitor *in vitro*. To further understand the molecular mechanism of amoxapine and its potential for treatment of CPT-11 induced diarrhea, we studied the binding modes of amoxapine and its metabolites by docking and molecular dynamics simulation, and tested the *in vivo* efficacy on mice in combination with CPT-11.

Experimental Design—The binding of amoxapine, its metabolites, 7-hydroxyamoxapine and 8-hydroxyamoxapine, and a control drug loxapine with GUS was explored by computational protocols. The *in vitro* potencies of metabolites were measured by *E. Coli* GUS enzyme and cell-based assay. Low dosage daily oral administration was designed to use along with CPT-11 to treat tumor-bearing mice.

Results—Computational modeling results indicated that amoxapine and its metabolites bound in the active site of GUS and satisfied critical pharmacophore features: aromatic features near bacterial loop residue F365' and hydrogen bond toward E413. Amoxapine and its metabolites were demonstrated as potent *in vitro*. Administration of low dosages of amoxapine with CPT-11 in mice achieved significant suppression of diarrhea and reduced tumor growth.

[*]**To whom correspondence should be addressed:** Hong Zhao, Department of Systems Medicine and Bioengineering, Houston Methodist Research Institute, Weill Cornell Medical College, 6670 Bertner Ave., R6-216, Houston, TX 77030, hzhao@houstonmethodist.org, Phone: 713-441-3557; Fax: 713-441-7189; John E. Scott, Biomanufacturing Research Institute and Technology Enterprise, North Carolina Central University, 1801 Fayetteville St., BRITE Bldg., Rm. 1019, Durham, NC 27707, jscott@nccu.edu, Phone: 919-530-7569.

Potential Conflicts of Interest:
A patent application has been filed related to the use of amoxapine to treat CPT-11 induced diarrhea (US Patent Application 20130345196).

Conclusions—Amoxapine has great clinical potential to be rapidly translated to human subjects for irinotecan induced diarrhea.

Keywords

amoxapine; β-glucuronidase; irinotecan (CPT-11); molecular docking and dynamics simulation; drug reposition

Introduction

Irinotecan (CPT-11) is a commonly used chemotherapeutic agent for the treatment of malignances, such as cancers of brain, colon and lung, and refractory forms of leukemia and lymphoma (1). However, 88% of patients receiving CPT-11 suffer from diarrhea, with 20-30% of them having severe diarrhea (CTCAE grades 3-4) (2). This side effect increases patient suffering and, more importantly, prevents dose intensification and efficacy in a significant fraction of patients undergoing irinotecan treatment (3). Some patients with severe diarrhea are forced to delay further treatment or stop therapy altogether. No effective therapy exists to overcome such diarrhea, and the USA the Food and Drug Administration (FDA) defines this situation as an unmet medical need (http://www.fda.gov).

The underlying mechanism of CPT-11 induced diarrhea has been extensively investigated. As a prodrug with a carbamate-linked dipiperidino moiety, CPT-11 is hydrolyzed by carboxylesterases (CES) *in vivo* to remove the dipiperidino group and it is then converted to its therapeutically active form SN-38. SN-38 inhibits type I DNA topoisomerase thereby killing rapidly proliferating tumor cells (4-5). SN-38 undergoes further metabolism in both liver and intestine by UDT-glucuronosyltransferase (UGT) which conjugates it with glucuronic acid to form the inactive SN-38G (6-7). This non-toxic form of the drug is then eliminated into gastrointestinal (GI) tract (8). In intestines, bacterial β-glucuronidase (GUS) enzymes in the microbiota, such as *Escherichia coli* (*E. coli*), remove the glucuronide group of SN-38G for a carbon source, regenerating cytotoxic SN-38 (9). Elimination of bacteria by antibiotics significantly reduced the SN-38 concentration in GI, showing the pivotal role of bacterial GUS (10). The accumulation of SN-38 in the intestinal lumen causes damage to intestinal epithelial cells and subsequently induces dose dependent diarrhea (11-12).

Given the essential role of bacterial GUS in the process of SN-38G reactivation, GUS inhibitor (GUSi) is expected to mitigate CPT-11 induced diarrhea. A GUS activity-based high-throughput assay has identified several compounds as potent bacterial GUS inhibitors (GUSis) (13-15). X-ray crystallography studies further revealed that the contacts between the inhibitors and a unique 17-residue “bacterial” loop lead to the selectivity of these compounds without affecting the mammalian GUS (13). Proof of concept studies have indicated that two of these compounds decreased the occurrence of diarrhea in mice receiving CPT-11 (13-14). However, these compounds will require prolonged lead optimization, *in vitro* and *in vivo* testing and high failure rate evaluations, including pharmacokinetic (PK)/pharmacodynamics (PD) studies and toxicity profiles for the single compound and in combination with CPT-11 before clinical trials can begin. Known drugs, having been used clinically, are believed to be good sources for new indications with clearly

understood safety and toxicity profiles (16). Therefore, we screened about 1,000 FDA-approved drugs for the ability to inhibit the enzymatic activity of purified bacterial GUS. The anti-depressant drug amoxapine (AMOX) was identified as a potent *in vitro* GUSi and determined to be one of the most promising potential drugs against bacterial GUS (17).

The chemical structure of amoxapine is different from previously reported GUS inhibitors, Inhibitor 1 and 2 (Supp. Fig. S1), but has similar potency for inhibiting GUS *in vitro* (17). As an old drug, amoxapine has known PK/PD properties and toxicity profile, which would facilitate its translation to human subjects. However, the *in vivo* efficacy of amoxapine against CPT-11 induced diarrhea remains unknown. 7-hydroxyamoxapine (7-OHAMOX) and 8-hydroxyamoxapine (8-OHAMOX) are the major metabolites of amoxapine (18). The metabolites may contribute to the *in vivo* efficacy. This motivated us to explore the exact binding mode of amoxapine and its metabolites with bacterial GUS, as well as the *in vitro* efficacy of the metabolites. According to the *in silico* and *in vitro* results, the administration of low dosage amoxapine along with CPT-11 was designed to treat tumor-bearing mice.

Materials and Methods

Computational details

Molecular Docking Protocol—The complex structure of bacterial GUS with Inhibitor 2 was taken from the Protein Data Bank (PDB) database (PDB ID: 3LPF) (13) and systematic operation was applied to get the tetramer, the functional unit of GUS. The two monomers which constitute the ligand binding site were kept in the following docking experiments as receptor. Glide 5.7 program from Schrodinger Suite was used to perform the docking experiments (19). Two water molecules forming hydrogen bonds with the natural ligand in the crystal structure were kept in the receptor. Then, the structure model was subjected to “Protein Preparation Wizard” workflow in Maestro (version 9.2) to assign hydrogens. The docking grid was generated using “Receptor Grid Generation” with center on the original ligand and internal size of 10 × 10 × 10 Å. The ligands were prepared using Ligprep 2.5 with MMFF force field from Schrodinger suite (19). Glide SP parameter set was applied in the docking protocol. The top ranking models by glide score were selected as the final binding mode.

Molecular Dynamics Simulation—The docking poses were used as the initial structure in MD simulation. The ligands were optimized at the Hartree-Fock level with the 6-31G (d,p) basis set using Gaussian 09 (20) and then restrained electrostatic potential (RESP) charges were calculated using the B3LYP/cc-pVTZ quantum mechanical method. The Amber ff99SB force field (21) and general Amber force field (GAFF) (22) were applied to proteins and ligands, respectively. All MD simulations were carried out using AMBER11(23) on BlueBiou of the IBM cluster at Rice University using 32 cores with the same protocol. Each simulation system was put in a truncated octahedron periodic box of SPC water molecules with a margin of 10.0 Å along each dimension, and sodium ions were added to maintain charge neutrality. All covalent bonds to hydrogen atoms were constrained using the SHAKE algorithm (24). Electrostatic interactions were calculated using the particle-mesh Ewald (PME) algorithm. A cutoff of 10 Å was applied to Lennard-Jones

interactions (25). 500 steps steepest-descent minimization followed by 1500 steps conjugated gradient minimization were applied to the system. Then it was heated up from 0 to 300 K gradually over 20 ps using the NVT ensemble with the solutes restrained by a weak harmonic potential. Afterward, 160 ps equilibrations were carried out in the NPT ensemble via three steps: the solutes were restrained while the waters and counter ions were equilibrated in the first 60 ps; then protein were relaxed in the next 20 ps; and all of the restraints were removed in the last 80 ps. Finally, the production MD simulations were conducted at 1 atm and 300 K under the NPT ensemble for 4 ns. Temperature was controlled using Langevin dynamics (26). The last 2 ns trajectory from production simulation was used to obtain the snapshots for MMPBSA free energy calculation (methods were described in supplementary materials) (27-29).

***In vitro* Enzyme and Cell-based assays—**Amoxapine, 7-hydroxyamoxapine and 8-hydroxyamoxapine were obtained from Sigma-Aldrich. *E. coli* DH5α (Zymo Research, Irvine, CA) was used for the cell-based assay. Purified *E. coli* GUS enzyme (cat No. G8420-25KU) was purchased from Sigma-Aldrich. All other reagents were obtained from Fisher Scientific. The assays were designed and performed as described in (17). For detailed information, see supplementary method section.

***In vivo* animal studies—**Irinotecan (CPT-11, Upjohn, Kalamazoo, MI) was purchased from LC Laboratories (#I-4122) as a hydrochloride salt (> 99% HPLC purified grade). CPT-11 was dissolved in ddH20 to make a stock of 20 mg/mL and stored at room temperature for a maximum of 2 hours prior to use. As vehicle control, all animals received an equivalent volume (compared to experimental groups) of 1% DMSO (ddH20) solution. Healthy 6-8 week old female Balb/cJ mice (000651) were obtained from Jackson Laboratories, Bar Harbor, ME. Mice were housed in conventional metabolic cages (N=1/cage). All studies were conducted in accordance with the guidelines of the Animal Care and Use Committee of Houston Methodist Research Institute.

The well-described CT-26 cell line, derived from a murine Balb/c colon adenocarcinoma, was used to make the tumor-bearing mouse model by s.c. injection of 0.02 ml cells in PBS at 5×10^7 cells/ml into the posterior mid-dorsum of mice (30). Tumor volumes were estimated by the formula $\pi/6 \times a^2 \times b$, where a is the short axis, and b the long axis. When tumor size reached ~500 mm^3 (~10 days after implantation, defined as day 1), mice were divided into five groups of 10-15 animals each: *(1) vehicle group*, vehicle controls received an equivalent volume of ddH_2O intraperitoneally (ip) and 1% DMSO by oral gavage (~100 μL twice per day); *(2) CPT-11 only group*, CPT-11 was injected (50 mg/kg) ip once daily in the morning with oral gavage of 1% DMSO (~100 μL twice per day) for 12 days; *(3) Amox-1 mg group*, amoxapine gavaged (0.5 mg/kg) twice per day (10 hours apart) for 12 days starting on day 1 with CPT-11 ip once per day; *(4) Amox-5 mg group*, amoxapine gavaged (2.5 mg/kg) twice per day (10 hours apart) for 12 days starting on day 1 with CPT-11 ip once per day; *(5) Inhibitor I group*, inhibitor I gavaged (0.5 mg/kg) twice per day (10 hours apart) for 12 days starting on day 1 with CPT-11 ip once per day. Inhibitor I was used as a control to compare the *in vivo* efficacy with amoxapine, and it is the closest analog

to inhibitor 2 and has been tested in animals (13) (Supp. Fig. S1). Total injected volume for drugs or vehicles was identical for each animal.

50 mg/kg CPT-11 in mice is roughly equivalent to the typical 5 mg/kg human CPT-11 dose based on differences in body surface area (BSA) (31-32). And 1 mg/kg and 5 mg/kg Amox in mice is approximately equivalent to 0.081and 0.243 mg/kg human equivalent dose (HED), respectively (33). Body weight, stool consistency and occult blood in stool were monitored daily using methods previously published (13). Mice were examined daily for signs of diarrhea (fecal staining of skin, lose watery stool) and bloody diarrhea (black sticky stool). After sacrifice, jejunum, ileum and colon samples were dissected. Tissues were formalin-fixed and paraffin embedded for histological examination using 6-μm-thick, 200-μm step serial sections stained with H&E, and a histologic score for each slide was calculated as described previously (13). For immunohistochemical staining, frozen slides at a thickness of 10μm were stained with antibodies against Ki67 and β-catenin overnight at 4°C. Slides were then washed and stained with the appropriate secondary antibodies. Mounted slides were examined under Olympus laser scanning confocal microscopy (FV1000, TMHRI Advanced Cellular and Tissue Microscope Core Facility).

Statistics—Statistical analysis was performed using SigmaPlot software (SigmaPlot for Windows, version 11.0). To determine the differences across multiple groups, one-way ANOVA was carried out. Independent two-sample t-test was conducted to detect difference in means between two groups. Data were summarized as means ± standard deviation (SD). $P<0.05$ was considered statistically significant.

Results

Analysis of Binding Modes obtained from docking

Similar to the Inhibitor 2 in 3LPF (PDB code) (13), all compounds bound at the entrance of the active site and make contacts with the residues from the primary monomer and F365' from the bacterial loop of the adjacent monomer (Fig. 1). The side chain of F365' is positioned parallel to the tricyclic aromatic ring of amoxapine and form a strong π-π interaction. L361 from the bacterial loop of the primary monomer, and F448/Y472 in the active site locate close to amoxapine and make strong hydrophobic contacts (Fig. 1A). The piperazine ring of amoxapine points into the active site with the amino moiety extending to within 2.7 Å of the catalytic E413 residue, forming strong hydrogen bond. The binding modes of the metabolites, 7-hydroxyamoxapine and 8-hydroxyamoxapine are very similar to that of amoxapine (Fig. 1B). Additional hydrogen bonds are found between the hydroxyl substitutions and the main-chain oxygen atom of F365'. However, for loxapine, having the substitution of methyl on the piperazine ring, no hydrogen bond is formed with E413 (Fig. 1C). The orientation of loxapine is totally different from that of amoxapine, with the methyl-piperazine pointing outside from the active site, and the tri-cyclic aromatic ring lying in the active site instead.

To compare the modes of amoxapine and Inhibitor 2, the docking pose of amoxapine and pose of Inhibitor 2 from the crystal structure are shown simultaneously in the active site in Fig 1.E. The dihydroquinoline ring of Inhibitor 2 almost overlaps with the tri-aromatic ring

from amoxapine, forming contacts with F365'. The piperazine ring of amoxapine extends deeper inside the active site and has a closer hydrogen bond distance with E413 (2.7Å) compared to that of the hydroxyl group of Inhibitor 2 (3.3Å). Key characters were extracted based on the binding mode of amoxapine and inhibitor 2: two aromatic ring pharmacophore features located in a parallel manner with F365' and hydrogen bond donor feature nearby E413 (Fig. 1F). Having both of the metabolites of amoxapine satisfying the pharmacophore model and even forming additional hydrogen bonds with mainchain of F365', it indicates that the activity of metabolites may be at a similar level as amoxapine or even more potent.

Molecular dynamics simulation and MMPBSA energy calculation

In order to refine the proposed binding modes from docking and evaluate the binding free energy, the complex structures of amoxapine, 7/8 hydroxyamoxapine and loxapine were taken as initial structures for molecular dynamics simulation. The RMSD of protein backbones are stable and around 2 Å in all the complex systems (Fig. 2). The average RMSD of amoxapine, 7-hydroxyamoxapine, 8-hydroxyamoxapine and loxapine in 4 ns is 2.67, 2.64, 2.41 and 4.59 Å, respectively. Dissociation of ligand was not observed in all the systems, but the RMSD for loxapine system is much larger than the others, which indicates reorientation and relocation occurred during the simulation. AMOX and 7/8 hydroxy metabolites conducted almost the same binding poses before and after the simulation, while loxapine moved a lot during the process (Supp. Fig. S2). The energetically unfavorable conformations usually result in a reorientation of the ligand or dissociation of the complex during the simulation. The high RMSD value and reorientation of loxapine implies unstable binding. Strong and stable hydrogen bonds were observed between amoxapine and the carboxyl side-chain of E413 during the simulation, as well as its metabolites (Supp. Table S1.). The occurrence time is over 60% and average distance around 2.8 Å. The hydrogen bond observed in the initial docking poses of metabolites with main chain of F365' was not maintained during the simulation.

Table 1 lists the energy items from the MMPBSA free energy calculation based on the MD simulation and the glide docking score based on the initial poses. In both the MMPBSA free energy calculation (ΔG_{MMPBSA}) and glide score, loxapine was ranked as the least potent compound in the table. It is consistent with our previous results from enzyme and cell based assays that loxapine shows no inhibition of bacterial GUS, with IC_{50} values > 100 μM. For loxapine, the desolvation cost (ΔG_{PB}) is particularly higher than the other molecules. In its initial docking pose, the tri-aromatic ring was located inside the active site composed by sidechains of several polar residues, E413, D163 and K562. The unfavorable hydrophobic ring in a polar environment may cause the highly increased electrostatic salvation energy, and finally the large increasing MMPBSA free energy for loxapine. 7/8-OHAMOX ranked as more potent than amoxapine in terms of glide score, however inversely via free energy. According to the computational results, we speculate that both of the metabolites may be active in the *in vitro* experiments.

Amoxapine and its metabolites are potent GUS inhibitors

Amoxapine and its metabolites were simultaneously tested in the GUS enzyme assay and cell-based GUS activity assay. AMOX, 7-OHAMOX and 8-OHAMOX generated IC50

values and SDs of 796 ± 29 nM, 981 ± 183 nM and 1,991 ± 275 nM, respectively, in the GUS enzyme assay (Fig. 3A). The cell-based assay involves the measurement of GUS enzymatic activity in live, intact *E. coli* bacteria. AMOX, 7-OHAMOX and 8-OHAMOX generated IC50 values and SDs of 58 ± 5 nM, 41 ± 6 nM and 100 ± 1 nM, respectively (Fig. 3B). A bacterial cytotoxicity assay using these same compounds indicated no toxicity to the bacterial cells at 2 and 20 μM (Fig. 3C). Thus, the activity of the AMOX and metabolites in the GUS cell-based assay was not due to killing of the bacteria. AMOX, 7-OHAMOX and 8-OHAMOX demonstrated 14-, 24-, and 20-fold, respectively, more potent activity in the cell-based GUS activity assay compared to the purified GUS enzyme assay. While this trend is unusual, it has been repeatedly observed for other GUSi compounds, but varies depending on the compound, with some compounds shifting less potent in the cell-based assay while others becoming more potent (13, 17). The 8-OHAMOX metabolite is somewhat less potent than AMOX, with about 2.5-fold higher IC50 in enzyme assay and 2-fold higher in the cell-based assay. However, both of the metabolites are active, having relatively low IC50 values. In addition, we previously demonstrated that amoxapine had no measurable IC50 against mammalian GUS (>100 μM IC50), thus resulting in a >100-fold selectivity for inhibiting bacterial GUS over mammalian GUS (17). With the 7 or 8 position substituted by hydroxyl, both of the metabolites retained the activity against bacterial GUS. The *in vitro* results are consistent with the computational modeling prediction and shows that not only AMOX, but also its major metabolites are potent GUS inhibitors.

Amoxapine successfully delayed or suppressed CPT-11-induced diarrhea in tumor-bearing mice

In our *in silico* and *in vitro* studies, both amoxapine and its metabolites show good potency against bacterial GUS. We thus conducted animal experiments to test the efficacy of amoxapine *in vivo*. Amoxapine was orally administered at 1mg/kg/day or 5mg/kg/day along with daily intraperitoneal (i.p.) CPT-11 treatment (the Amox group) in tumor-bearing mice. Signs of diarrhea exhibited in mice were most apparent by residual staining around the anus. Diarrhea was first observed on day 7 of daily CPT-11 treatment with 50% of the mice from the CPT-11 group exhibiting diarrhea, while 10% of the Amox-1mg group had diarrhea (Fig. 4A). Peak efficacy was apparent on day 8 when 65% of the mice from the CPT-11 group exhibited diarrhea staining compared to only 10% of the mice in the Amox-1mg group. By day 9, 90% of the CPT-11 mice had diarrhea compared to 50% of Amox-1mg group. The Amox-5mg treatment totally prevented the appearance of diarrhea on day 7, and on days 8 and 9, only 20% and 30% of the mice, respectively, in the Amox-5mg group showed diarrhea. 30% of the mice in both the amoxapine groups never showed diarrhea during the course of the entire study, and the body weight of the survived mice showed rapid recovery (about 50% of the lost weight) 4 days after the cessation of CPT-11. The previously published GUSi Inhibitor 1 (13) was also included in this study as a positive control. Overall, amoxapine (1 or 5 mg/kg) had similar efficacy as Inhibitor 1 in suppressing diarrhea (Fig. 4A). In addition, diarrhea staining in the CPT-11 group was much more severe than diarrhea staining in the Amox groups. Staining in mice from the CPT-11 group was darker (bloodier) and more liquid, and consequently, all mice in the CPT-11 group had to be euthanized before or on day 12. Mice in the Amox-5mg group had a significant delay on the euthanization survival plot (p=0.004, log-rank test) (Fig. 4B), even more of a delay than the

Inhibitor 1 control. Thus, in addition to the frequency of diarrhea being reduced, the euthanization data indicated that the severity of diarrhea was also attenuated by amoxapine.

Histological examination of the jejunum, ileum and colon indicated that all tissue samples from CPT-11-treated mice demonstrated moderate to severe damage, as shown in Fig. 5A. Tightly arrayed epithelial cells were displayed in the vehicle group samples, whereas obvious short villi and crypt loss, or even a complete abolishment of the top villi along with a large influx of inflammatory cells and significant fibrosis were observed in jejunum and ilenum in damaged intestines (Fig. 5A). In comparison with the damage in the small intestine, the morphology of colon tissues in CPT-11-treated mice showed similar changes (Fig. 5A). In contrast, oral administration of amoxapine protected the glandular structure of the intestinal and colon tissues (Fig. 5A) (Supp. Table S2). The protective effect of amoxapine was further studied by immufluorescence staining using the proliferative marker Ki67 and cell membrane marker β-catenin (Fig.5B-C). Severe proliferative cell loss was observed in CPT-11-treated mice, implying a difficult recovery from the damage, in accordance with the loss of cell membrane integrity. However, co-treatment of amoxapine with CPT-11 facilitated a significant increase of proliferative cells and maintained the integrity of the top epithelial cell membrane (Fig. 5B-C, Supp. Table. S2). These results indicate convincing *in vivo* efficacy of amoxapine in suppressing diarrhea in CPT-11-treated mice.

Co-treatment of amoxapine and CPT-11 in reducing tumor growth

Co-treatment of amoxapine and CPT-11 yielded positive results in reducing average tumor growth (Fig. 4C). Throughout the experiment, the average tumor size of mice in the Amox-1mg group was as low as, if not lower than, the average tumor size of CPT-11 group mice. This data suggested that the 1mg/kg dose of amoxapine, which possessed anti-diarrhea efficacy, had absolutely no effect on diminishing the tumor-killing ability of CPT-11. Furthermore, mice in the Amox-5mg group showed significantly lower tumor size than the average tumor size of CPT-11 group mice ($p=0.015$, two-way ANOVA) (Fig. 4C), suggesting possible enhanced efficacy for reducing tumor size by the combination of amoxapine and CPT-11.

Discussion

For the first time, we report that the antidepressant drug amoxapine has the potential to be repositioned as a new potent and selective bacterial GUS inhibitor that alleviates irinotecan-associated diarrhea. The binding mode of AMOX is exhibited at the atomic level by using molecular docking and dynamics simulations. AMOX binds in the same active site of GUS as Inhibitor 2 in crystal structure (17) and shares common pharmacophore features: two aromatic features near bacterial loop residue F365’ and one hydrogen bond donor feature toward E413, but with different chemical patterns. As a result of such binding with GUS, *in vitro* assays of amoxapine showed potent inhibition of GUS activity. Furthermore, the two metabolites with similar binding modes showed strong *in vitro* GUS inhibitory activity and likely contributed to *in vivo* efficacy.

Severe late stage diarrhea, caused by intestinal SN-38, frequently occurs in patients treated with CPT-11. The current recommended treatment for this diarrhea is loperamide or antibiotics (34). However, loperamide only treats the symptoms while tissue damage still occurs, and it is not recommended for more than 48 hours due to the risk of paralytic ileus (Pfizer, Inc. (2012). CAMPTOSAR, New York). Antibiotics kill the intestinal biota, which is important in carbohydrate metabolism, vitamin production and the processing of bile acids, sterols and xenobiotics; they are not optimal for the patients already challenged by tumor growth and chemotherapy (35-36). There are active clinical trials in testing drugs to prevent or suppress such diarrhea, but no positive results have been published (clinicaltrials.gov identifier: NCT00037180, NCT01410955, NCT00255229, NCT00040391, NCT00006269, NCT00143533, NCT00582426). GUSis are expected to fit the therapeutic need for several reasons. First, a GUSi would inhibit the intestinal regeneration of SN-38 from SN-38G to alleviate diarrhea via blocking the bacteria GUS. Concerns may arise that decreasing the SN-38 concentration in intestinal lumen may weaken the anti-tumor efficacy of CPT-11. However, SN-38 in feces of cancer patient was only 2.45 ± 1.16% of the total administrated CPT-11 (11). Thus re-absorption of SN-38 from intestines may not contribute significantly to plasma concentration. Moreover, blocking the SN-38 intestinal absorption in patients by using oral alkalization showed no decrease on the tumor response rates (37). To date, intestinal SN-38 has been reported to associate with only toxicity, not efficacy. Second, GUSis would not kill the commensal bacteria essential for human health and avoid potential complications of using antibiotics, including allergies. Third, reduction in the diarrhea side-effect may allow dose intensification of CPT-11 above what is currently used and thus enhance anti-tumor efficacy.

Amoxapine is identified as a potent and selective GUSi that may satisfy the aforementioned criteria. In addition, amoxapine has further advantages to strengthen the case for repositioning it for this new indication. Co-treatment of 5 mg/kg amoxapine with CPT-11 yielded enhanced effect in reducing tumor growth in mice, which was not found in mice treated with Inhibitor 1 (Fig. 4C). We speculate that the observed enhanced anti-tumor efficacy may lie in the non-competitive P-glycoprotein inhibitor property of amoxapine (38). P-glycoprotein is located on cell membrane and pumps foreign substances out of cells. Acquired tumor cell resistance to CPT-11 and SN-38 has been observed due to the drug transporter P-glycoprotein (39). Amoxapine may block the P-glycoprotein, lead to the accumulation of SN-38 in the cell, and thus increase the cell apoptosis and anti-tumor efficacy. However, the effect of amoxapine on tumor growth needs to be eventually confirmed in additional experiments with other xenograft models. Beside the enhanced anti-tumor efficacy, the dosages of amoxapine for preventing the diarrhea in mice was notably as low as 1mg/kg/day and 5mg/kg/day, with the human equivalent dose (HED) calculated as 0.081-0.243mg/kg (33). It is roughly 6~8 fold lower than the minimal initial dose of amoxapine used for depression treatment in clinic. We expect low doses for patients to avoid new side effects or psychological effects, and at the same time, achieve the diarrhea suppression. It should be noted that the extrapolation to an active human dose of amoxapine based on allometric scaling is imprecise. The dosage and resulting safety threshold would need to be determined in future work. Nevertheless, as an old drug, amoxapine has been carefully evaluated for side effects and toxicity in human body and its PK/PD properties

have been comprehensively studied. It has the advantage to be translated to patients in a relatively short period compared to the *de novo* discovered compounds (e.g. Inhibitor 1 or 2).

Amoxapine is an FDA approved drug and has been used in treatment of major depressive disorder since 1992 (40). The behavior of amoxapine in human subjects is clearly described in the literature (18, 41-42). Amoxapine is rapidly absorbed and metabolized after oral administration, and maximum plasma concentration is achieved for AMOX, 7-OHAMOX and 8-OHAMOX in 0.5 h, 1 h and 3 h, respectively. The level of 8-OHAMOX is significantly higher than that of AMOX or 7-OHAMOX in plasma. The area under the curve value for 8-OHAMOX was three to five times greater than that for AMOX. The mean elimination half-lives for AMOX, 7-OHAMOX and 8-OHAMOX are 9.8h, 5.1h and 30.8 h, respectively. With the highest plasma concentration and longest half-life, 8-OHAMOX is the major existing form of AMOX *in vivo* by oral administration. The *in silico* and *in vitro* results showed that both 7-OHAMOX and 8-OHAMOX are potent GUS inhibitors, which likely contributed to the efficacy of AMOX against diarrhea *in vivo*. In both groups of AMOX, 1 mg/kg/day and 5 mg/kg/day orally in combination with CPT-11(IP), significant suppression of severe diarrhea was observed starting on day 7 (Fig. 4C). About 30% of the mice receiving amoxapine never showed diarrhea during the course of the study.

Despite the observed efficacy, it is noted that the diarrhea could not be fully abrogated by amoxapine. The best anti-diarrhea effects of amoxapine were achieved on day 7-9, but at day 12, 70% of the mice still progressed to severe diarrhea. Interestingly, this phenomenon was the same for the mice receiving Inhibitor 1 treatment (13). It should be noted that GUS is not the only factor leading to the diarrhea. The intestine in both humans and rodents is also rich in carboxylesterase (CES) and UGT enzymes. CES hydrolyzes the CPT-11 to SN-38, while the UGT enzyme undertakes the detoxification of SN-38 to SN-38G (4, 6-7). The possible reason for accumulation of SN-38 in the presence of GUSi may lie in two aspects, the continuous conversion from CPT-11 to SN-38 by CES, and the incomplete transformation of SN-38 to SN-38G by UGT. GUSi is useless for the SN-38 that already exists in the GI other than the one regenerated from SN-38G by the bacterial GUS. These *in vivo* outcomes may be precisely controlled through the complicated manipulation of CES, UGT and GUS. As the intestinal CES2 exhibits a higher affinity and velocity than hepatic CES1, it is suggested as a new clinical target to minimize CPT-11 induced diarrhea (43-45). The intestinal CES inhibitors working together with GUSi may achieve an improved therapeutic outcome for CPT-11 induced diarrhea. Moreover, the next step to strengthen the efficacy may be to reformulate AMOX as a slow-gut-release form to directly expose it to bacteria and improve the local compound concentration in intestine.

In conclusion, amoxapine and its metabolites are potent and selective GUS inhibitors binding in the active site near the bacterial loop. Significant suppression of diarrhea was obtained by combining the administration of amoxapine and CPT-11 in xenograft model mice, as well as improved efficacy in reducing tumor growth. As an old drug with known pharmaceutical properties and toxicity profile, amoxapine has great clinical potential to be transferred to human subjects in order to prevent CPT-11 induced diarrhea with minimal side effects and even strengthen the efficacy of this chemotherapy.

Supplementary Material

Refer to Web version on PubMed Central for supplementary material.

Acknowledgments

We thank James Mancuso for proofreading the manuscript. The microscopic imaging experiments were performed at Houston Methodist Research Institute's Advanced Cellular and Tissue Microscope Core Facility. The authors are grateful for high performance computing resources provide by BlueBioU in Rice University. A patent application has been filed related to the use of amoxapine to treat CPT-11 induced diarrhea (US Patent Application 20130345196).

Financial support: This research is funded by John S. Dunn Research Foundation (STCW) in Houston Methodist Hospital and National Institutes of Health (NIH) grant U54CA156735 (JES), as well as in part by a grant from the Golden LEAF Foundation (JES) and funds from the State of North Carolina (JES).

References

1. Pommier Y. Topoisomerase I inhibitors: camptothecins and beyond. Nat Rev Cancer. 2006; 6:789–802. [PubMed: 16990856]
2. Tam VC, Rask S, Koru-Sengul T, Dhesy-Thind S. Generalizability of toxicity data from oncology clinical trials to clinical practice: toxicity of irinotecan-based regimens in patients with metastatic colorectal cancer. Curr Oncol. 2009; 16:13–20. [PubMed: 20016742]
3. Abigerges D, Armand J-P, Chabot GG, Costa LD, Fadel E, Cote C, et al. Irinotecan (CPT-11) High-Dose Escalation Using Intensive High-Dose Loperamide to Control Diarrhea. Journal of the National Cancer Institute. 1994; 86:446–9. [PubMed: 8120919]
4. Satoh T, Hosokawa M, Atsumi R, Suzuki W, Hakusui H, Nagai E. Metabolic activation of CPT-11, 7-ethyl-10-[4-(1-piperidino)-1-piperidino]carbonyloxycamptothecin, a novel antitumor agent, by carboxylesterase. Biol Pharm Bull. 1994; 17:662–4. [PubMed: 7920428]
5. Kawato Y, Aonuma M, Hirota Y, Kuga H, Sato K. Intracellular roles of SN-38, a metabolite of the camptothecin derivative CPT-11, in the antitumor effect of CPT-11. Cancer Res. 1991; 51:4187–91. [PubMed: 1651156]
6. Iyer L, King CD, Whitington PF, Green MD, Roy SK, Tephly TR, et al. Genetic predisposition to the metabolism of irinotecan (CPT-11). Role of uridine diphosphate glucuronosyltransferase isoform 1A1 in the glucuronidation of its active metabolite (SN-38) in human liver microsomes. J Clin Invest. 1998; 101:847–54. [PubMed: 9466980]
7. Chen S, Yueh MF, Bigo C, Barbier O, Wang K, Karin M, et al. Intestinal glucuronidation protects against chemotherapy-induced toxicity by irinotecan (CPT-11). Proc Natl Acad Sci U S A. 2013
8. Kaneda N, Yokokura T. Nonlinear pharmacokinetics of CPT-11 in rats. Cancer Res. 1990; 50:1721–5. [PubMed: 2306726]
9. Takasuna K, Hagiwara T, Hirohashi M, Kato M, Nomura M, Nagai E, et al. Involvement of beta-glucuronidase in intestinal microflora in the intestinal toxicity of the antitumor camptothecin derivative irinotecan hydrochloride (CPT-11) in rats. Cancer Res. 1996; 56:3752–7. [PubMed: 8706020]
10. Takasuna K, Hagiwara T, Hirohashi M, Kato M, Nomura M, Nagai E, et al. Inhibition of intestinal microflora beta-glucuronidase modifies the distribution of the active metabolite of the antitumor agent, irinotecan hydrochloride (CPT-11) in rats. Cancer Chemother Pharmacol. 1998; 42:280–6. [PubMed: 9744772]
11. Sparreboom A, de Jonge MJ, de Bruijn P, Brouwer E, Nooter K, Loos WJ, et al. Irinotecan (CPT-11) metabolism and disposition in cancer patients. Clin Cancer Res. 1998; 4:2747–54. [PubMed: 9829738]
12. Hu ZP, Yang XX, Chan SY, Xu AL, Duan W, Zhu YZ, et al. St. John's wort attenuates irinotecan-induced diarrhea via down-regulation of intestinal pro-inflammatory cytokines and inhibition of intestinal epithelial apoptosis. Toxicol Appl Pharmacol. 2006; 216:225–37. [PubMed: 17015070]

13. Wallace BD, Wang H, Lane KT, Scott JE, Orans J, Koo JS, et al. Alleviating cancer drug toxicity by inhibiting a bacterial enzyme. Science. 2010; 330:831–5. [PubMed: 21051639]
14. Roberts AB, Wallace BD, Venkatesh MK, Mani S, Redinbo MR. Molecular Insights into Microbial β-Glucuronidase Inhibition to Abrogate CPT-11 Toxicity. Molecular Pharmacology. 2013; 84:208–17. [PubMed: 23690068]
15. Ahmad S, Hughes MA, Lane KT, Redinbo MR, Yeh LA, Scott JE. A High Throughput Assay for Discovery of Bacterial beta-Glucuronidase Inhibitors. Curr Chem Genomics. 2011; 5:13–20. [PubMed: 21643506]
16. Chong CR, Sullivan DJ Jr. New uses for old drugs. Nature. 2007; 448:645–6. [PubMed: 17687303]
17. Ahmad S, Hughes MA, Yeh L-A, Scott JE. Potential Repurposing of Known Drugs as Potent Bacterial β-Glucuronidase Inhibitors. Journal of Biomolecular Screening. 2012; 17:957–65. [PubMed: 22535688]
18. Calvo B, Garcia MJ, Pedraz JL, Marino EL, Dominguez-Gil A. Pharmacokinetics of amoxapine and its active metabolites. Int J Clin Pharmacol Ther Toxicol. 1985; 23:180–5. [PubMed: 3997304]
19. Schrodinger. Schrodinger, LLC; New York, NY: 2011. 2011.
20. Frisch, MJ.; Trucks, GW.; Schlegel, HB.; Scuseria, GE.; Robb, MA.; Cheeseman, JR., et al. Gaussian 09, Revision A.1. Gaussian, Inc.; Wallingford CT: 2009.
21. Hornak V, Abel R, Okur A, Strockbine B, Roitberg A, Simmerling C. Comparison of multiple Amber force fields and development of improved protein backbone parameters. Proteins. 2006; 65:712–25. [PubMed: 16981200]
22. Wang J, Wolf RM, Caldwell JW, Kollman PA, Case DA. Development and testing of a general amber force field. J Comput Chem. 2004; 25:1157–74. [PubMed: 15116359]
23. Case TAD, DA.; Cheatham, TE., III; Simmerling, CL.; Wang, J.; Duke, RE.; Luo, R.; Walker, RC.; Zhang, W.; Merz, KM.; Roberts, B.; Wang, B.; Hayik, S.; Roitberg, A.; Seabra, G.; Kolossvai, I.; Wong, KF.; Paesani, F.; Vanicek, J.; Liu, J.; Wu, X.; Brozell, SR.; Steinbrecher, T.; Gohlke, H.; Cai, Q.; Ye, X.; Wang, J.; Hsieh, M-J.; Cui, G.; Roe, DR.; Mathews, DH.; Seetin, MG.; Sagui, C.; Babin, V.; Luchko, T.; Gusarov, S.; Kovalenko, A.; Kollman, PA. AMBER 11. University of California; San Francisco:
24. Ryckaert J, Ciccotti G, Berendsen H. Numerical integration of the cartesian equations of motion of a system with constraints: molecular dynamics of n-alkanes. Journal of Computational Physics. 1977; 23:327–41.
25. Darden T, York D, Pedersen L. Particle mesh Ewald: An N [center-dot] log(N) method for Ewald sums in large systems. The Journal of Chemical Physics. 1993; 98:10089–92.
26. Izaguirre J, Catarello D, Wozniak J, Skeel R. Langevin stabilization of molecular dynamics. The Journal of Chemical Physics. 2001; 114:2090–8.
27. Hou T, Wang J, Li Y, Wang W. Assessing the performance of the MM/PBSA and MM/GBSA methods. 1. The accuracy of binding free energy calculations based on molecular dynamics simulations. J Chem Inf Model. 2011; 51:69–82. [PubMed: 21117705]
28. Yang T, Wu JC, Yan C, Wang Y, Luo R, Gonzales MB, et al. Virtual screening using molecular simulations. Proteins: Structure, Function, and Bioinformatics. 2011; 79:1940–51.
29. Kollman PA, Massova I, Reyes C, Kuhn B, Huo S, Chong L, et al. Calculating Structures and Free Energies of Complex Molecules: Combining Molecular Mechanics and Continuum Models. Accounts of Chemical Research. 2000; 33:889–97. [PubMed: 11123888]
30. Zhao J, Huang L, Belmar N, Buelow R, Fong T. Oral RDP58 allows CPT-11 dose intensification for enhanced tumor response by decreasing gastrointestinal toxicity. Clin Cancer Res. 2004; 10:2851–9. [PubMed: 15102694]
31. Brandi G, Dabard J, Raibaud P, Di Battista M, Bridonneau C, Pisi AM, et al. Intestinal microflora and digestive toxicity of irinotecan in mice. Clin Cancer Res. 2006; 12:1299–307. [PubMed: 16489087]
32. Reagan-Shaw S, Nihal M, Ahmad N. Dose translation from animal to human studies revisited. FASEB J. 2008; 22:659–61. [PubMed: 17942826]
33. Reagan-Shaw S, Nihal M, Ahmad N. Dose translation from animal to human studies revisited. The FASEB Journal. 2008; 22:659–61.

34. de Jong FA, Kehrer DFS, Mathijssen RHJ, Creemers G-J, de Bruijn P, van Schaik RHN, et al. Prophylaxis of Irinotecan-Induced Diarrhea with Neomycin and Potential Role for UGT1A1*28 Genotype Screening: A Double-Blind, Randomized, Placebo-Controlled Study. The Oncologist. 2006; 11:944–54. [PubMed: 16951398]
35. Cummings JH, Macfarlane GT. Role of intestinal bacteria in nutrient metabolism. JPEN J Parenter Enteral Nutr. 1997; 21:357–65. [PubMed: 9406136]
36. Guarner F, Malagelada JR. Gut flora in health and disease. Lancet. 2003; 361:512–9. [PubMed: 12583961]
37. Takeda Y, Kobayashi K, Akiyama Y, Soma T, Handa S, Kudoh S, et al. Prevention of irinotecan (CPT-11)-induced diarrhea by oral alkalization combined with control of defecation in cancer patients. Int J Cancer. 2001; 92:269–75. [PubMed: 11291056]
38. Palmeira A, Rodrigues F, Sousa E, Pinto M, Vasconcelos MH, Fernandes MX. New uses for old drugs: pharmacophore-based screening for the discovery of P-glycoprotein inhibitors. Chem Biol Drug Des. 2011; 78:57–72. [PubMed: 21235729]
39. Jansen WJ, Hulscher TM, van Ark-Otte J, Giaccone G, Pinedo HM, Boven E. CPT-11 sensitivity in relation to the expression of P170-glycoprotein and multidrug resistance-associated protein. Br J Cancer. 1998; 77:359–65. [PubMed: 9472629]
40. Ban TA, Wilson WH, McEvoy JP. Amoxapine: a review of literature. Int Pharmacopsychiatry. 1980; 15:166–70. [PubMed: 7016801]
41. Cooper TB, Kelly RG. GLC analysis of loxapine, amoxapine, and their metabolites in serum and urine. Journal of Pharmaceutical Sciences. 1979; 68:216–9. [PubMed: 423094]
42. Takeuchi H, Yokota S, Shimada S, Ohtani Y, Miura S, Kubo H. Pharmacokinetics of amoxapine and its active metabolites in healthy subjects. Current therapeutic research, clinical and experimental. 1993; 53:427–34.
43. Khanna R, Morton CL, Danks MK, Potter PM. Proficient metabolism of irinotecan by a human intestinal carboxylesterase. Cancer Res. 2000; 60:4725–8. [PubMed: 10987276]
44. Humerickhouse R, Lohrbach K, Li L, Bosron WF, Dolan ME. Characterization of CPT-11 hydrolysis by human liver carboxylesterase isoforms hCE-1 and hCE-2. Cancer Res. 2000; 60:1189–92. [PubMed: 10728672]
45. Wadkins RM, Hyatt JL, Yoon KJ, Morton CL, Lee RE, Damodaran K, et al. Discovery of novel selective inhibitors of human intestinal carboxylesterase for the amelioration of irinotecan-induced diarrhea: synthesis, quantitative structure-activity relationship analysis, and biological activity. Mol Pharmacol. 2004; 65:1336–43. [PubMed: 15155827]

Translational Relevance

Irinotecan (CPT-11) is a cytotoxic drug that has wide applicability and usage in cancer treatment. Despite its success, patients suffer dose-dependent diarrhea, limiting the drug's efficacy. No effective therapy is available for this unmet medical need. Bacteria β-glucuronidase (GUS) enzyme in the intestines plays a pivotal role in CPT-11 induced diarrhea via reactivating the non-tox CPT-11 metabolite, SN-38G, back to toxic SN-38. Here, we report the molecular mechanism for an identified GUS inhibitor (GUSi) amoxapine and the corresponding animal studies using amoxapine in combination with CPT-11. Because amoxapine metabolites are potent GUSis, the use of amoxapine significantly delayed or suppressed diarrhea *in vivo* at a dose remarkably lower than normal use. Rapid translation to human subjects may be achievable for this old drug to alleviate CPT-11 drug toxicity and improve efficacy.

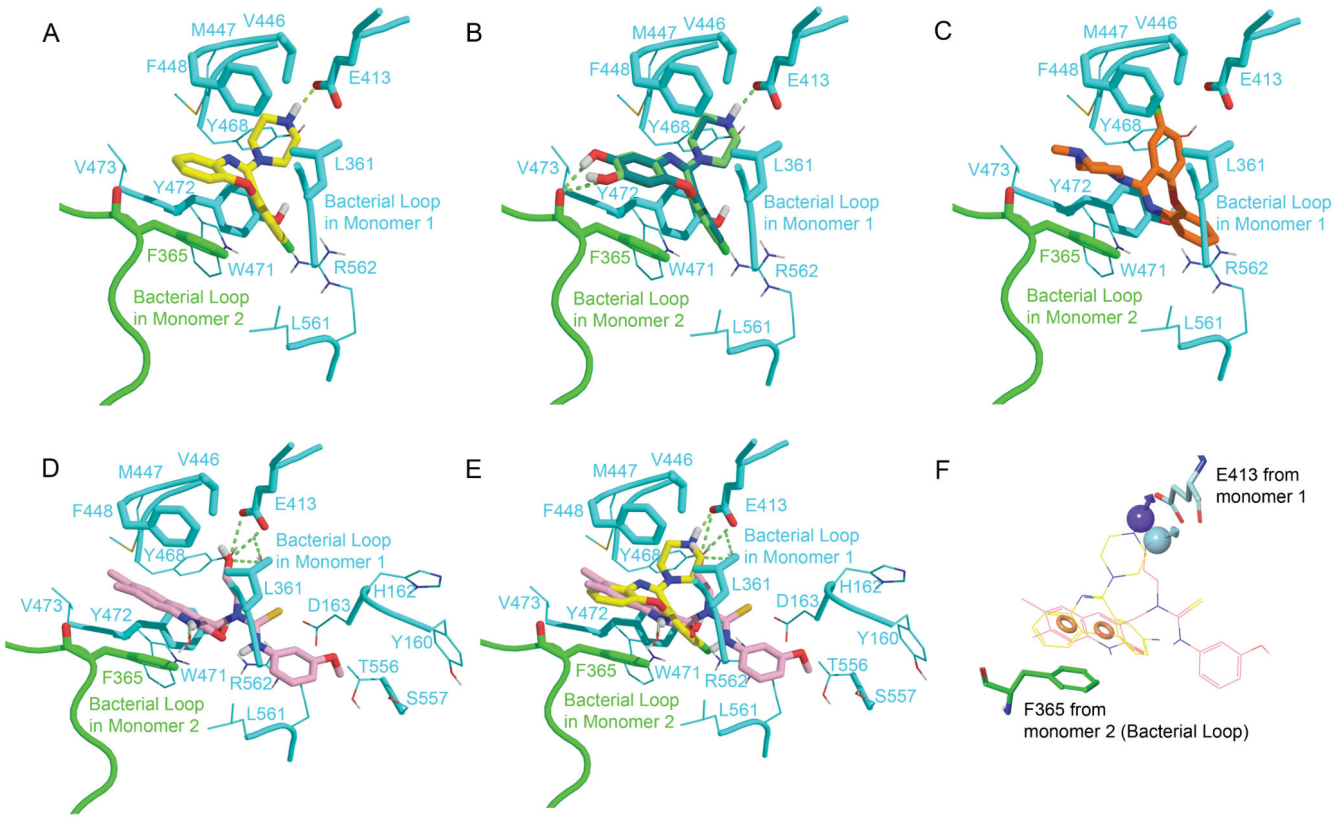

Fig. 1. Binding modes of A, amaxapine (yellow); B, 7-hydroxyamoxapine (lime) and8-hydroxyamoxapine (dark green); C, loxapine (orange); D, Inhibitor 2 (pink) from 3LPF; E, Amoxapine and Inhibitor 2 in the same active site; F, Pharmacophore features for Amoxapine and Inhibitor 2

The compounds and close contacting residues are shown in sticks. Residues in 5 Å around the ligands depicted the active site are shown in lines. The primary monomer is colored in cyan and bacterial loop from the adjacent monomer is colored in green. The hydrogen bonds are drawn in lime dash lines. In the mode of loxapine, the critical hydrogen bond with E413 is missing. The pharmacophore based on amoxpine and Inhibitor 2 is composed by two aromatic ring features (shown in orange spheres) and hydrogen bond donors pointed to E413 (purple and cyan spheres).

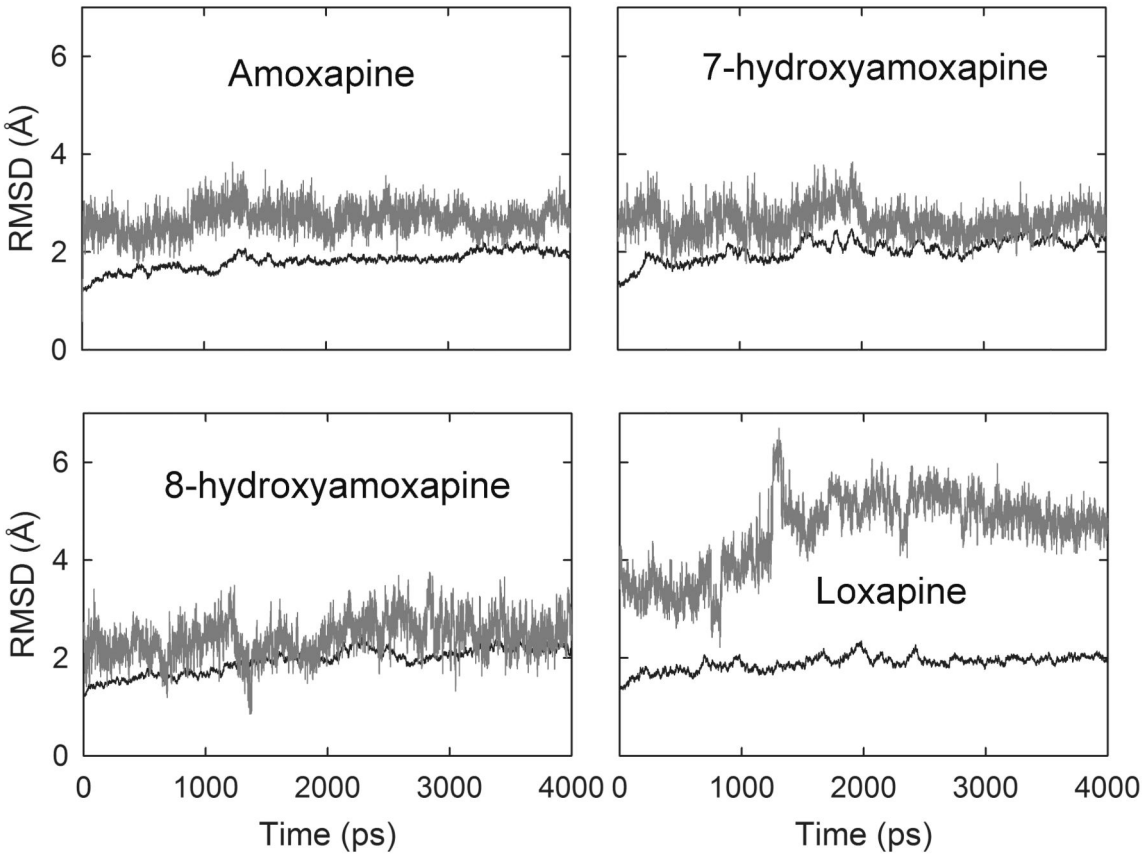

Fig. 2. Root mean square deviation (RMSD) of protein backbone atoms (black) and ligand (gray) with respect to time over 4 ns MD simulation for four complex systems

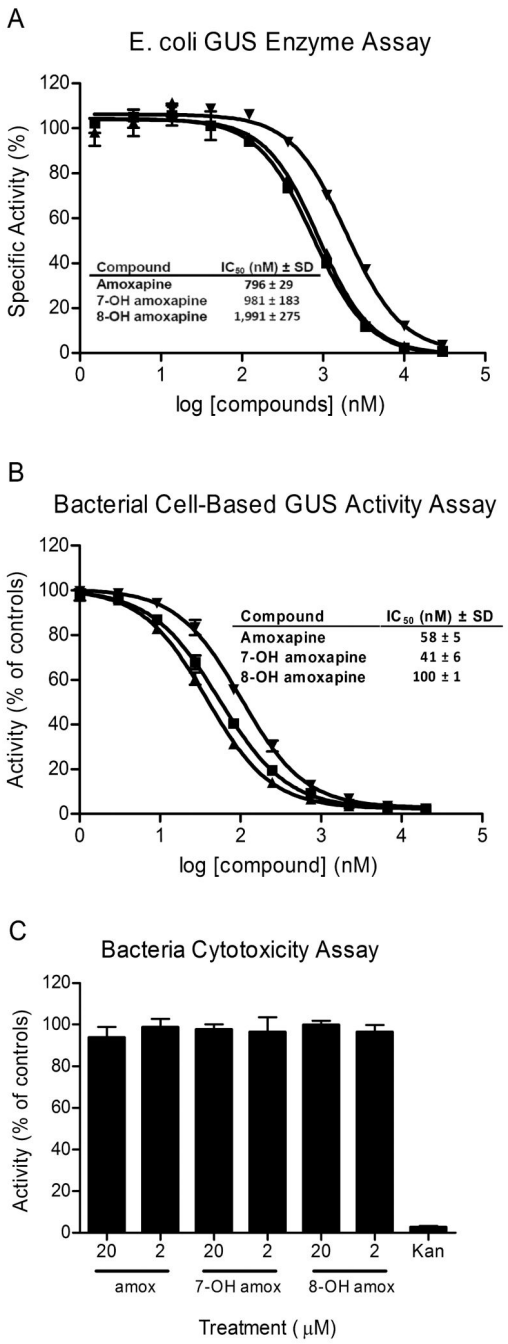

Fig. 3. *In vitro* potency determinations for amoxapine and its metabolites

IC_{50} values provided in the tables are average values based on three independent determinations along with standard deviations (SD). (**A**) IC_{50} value determinations were performed for amoxapine (■), 7-OH amoxapine (▲) and 8-OH amoxapine (▼) using the GUS enzyme assay. The indicated concentrations were tested in duplicate and activity was normalized to control wells (± enzyme). (**B**) IC_{50} value determinations were performed for amoxapine (■), 7-OH amoxapine (▲) and 8-OH amoxapine (▼) using the bacterial cell-based GUS activity assay. The indicated concentrations were tested in duplicate and activity

was normalized to control wells (± bacteria). (**C**) The indicated compounds were tested in the bacterial cytotoxicity assay at 20 and 2 μM, as indicated. The compounds were tested in triplicate at these concentrations and activity was normalized to control wells (± bacteria). The antibiotic kanamycin (Kan) was included as a positive control. Data points represent the average of two or three determinations per variable and error bars represent SD. Data shown are representative of three independent experiments.

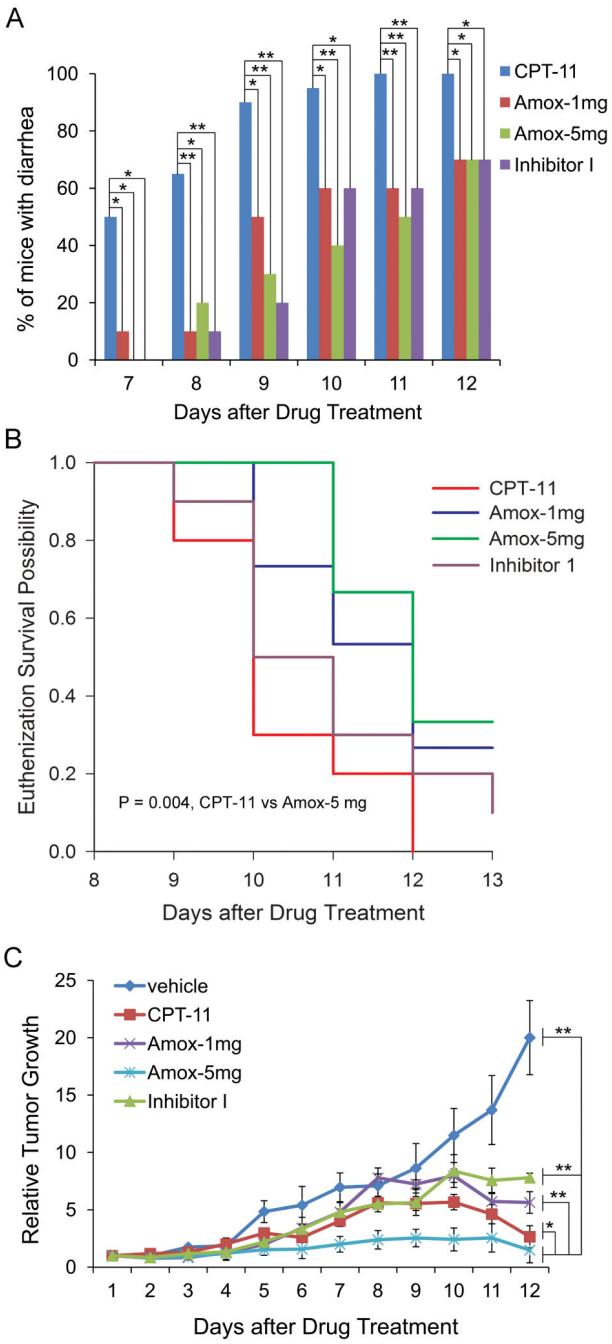

Fig. 4. Effects of Amoxapine on CPT-11-induced diarrhea, survival and tumor growth in tumor-bearing mice

A, Amoxapine treatment successfully delayed or suppressed CPT-11-induced diarrhea in tumor-bearing mice. Amoxapine 1mg/kg/day (Amox-1mg) or 5mg/kg/day (Amox-5mg), or inhibitor I 1mg/kg/day (Inhibitor-I) was orally administered twice per day along with daily i.p. CPT-11 treatment. N=15 mice per group. * $p<0.05$; ** $p<0.01$, by Fisher Exact Test. **B,** Amoxapine treatment improved the survival of CPT-11-treated tumor-bearing mice. By the Log-rank test, CPT-11 vs. Amox-5mg, p=0.004. **C,** Amoxapine in combination with

CPT-11 achieved addictive effect in suppressing tumor growth. Amoxapine was gavaged at 1mg/kg/day or 5mg/kg/day for 12 days with daily i.p. injection of CPT-11. Tumor volumes were estimated by the formula $\pi/6 \times a^2 \times b$, where a is the short axis, and b the long axis. * $p<0.05$; ** $p<0.01$, by Two-way ANOVA analysis, taking time and group as factors. Sigma Plot software was used to calculate the P value.

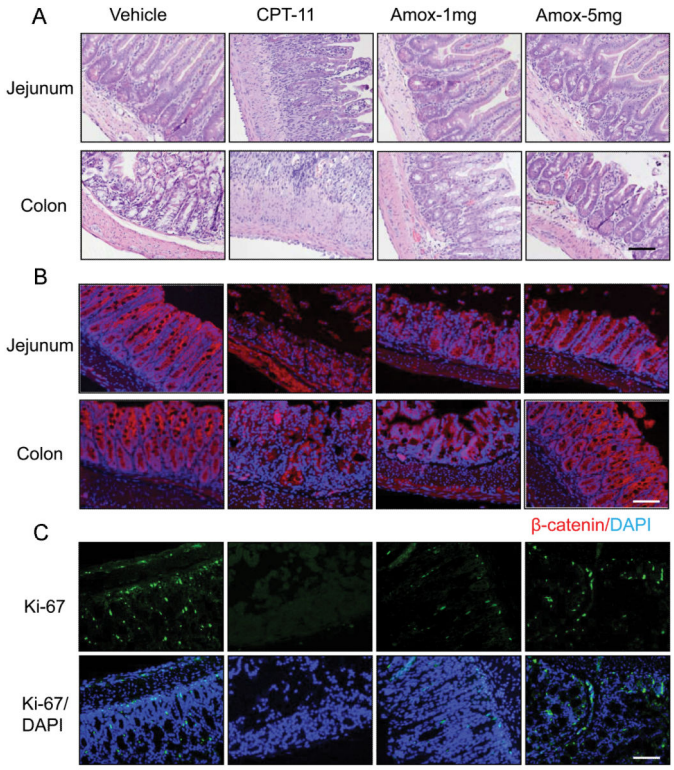

Fig. 5. Amoxapine protected the CPT-11 induced intestinal damage in tumor-bearing mice

Intestine tissues from the CPT-treated mice were analyzed after 8 consecutive days of treatment with amoxapine 1mg/kg/day (Amox-1mg) or 5mg/kg/day (Amox-1mg). The representative images of H&E staining (A), immunohistological staining of β-catenin on the integrity of cell membrane (B), and Ki-67 on the proliferative cells (C) of the jejunum and colon are photographed. Scale bar: 100μm.

Table 1

Binding free energies[a] of Amoxapine, its metabolites, and Loxapine with bacterial β-glucuronidase

Ligand	ΔE_{vdw}	$\Delta E_{electrostatic}$	ΔG_{gas}	ΔG_{PB}	ΔG_{SA}	$\Delta G_{solvent}$	$\Delta G_{electrostatic}$[b]	ΔG_{np}[c]	ΔG_{MMPBSA}	Glide score[d]
AMOX	−42.41	−7.42	−49.82	23.27	−2.82	20.45	15.85	−45.23	−29.38	−8.09
7-OHAMOX	−39.58	−7.28	−46.86	25.16	−2.74	22.43	17.88	−42.32	−24.44	−8.33
8-OHAMOX	−38.92	−13.07	−51.99	34.06	−3.09	30.97	20.99	−42.01	−21.02	−8.59
Loxapine	−45.48	−9.84	−55.32	47.49	−3.49	44.01	37.65	−48.97	−11.32	−7.68

[a] All the energies are in kcal/mol; Snapshots extracted from the last 2 ns MD simulation were submitted to MMPBSA.py for the free energy calculation.

[b] Total electrostatic contribution: $\Delta G_{electrostatic} = \Delta E_{electrostatic} + \Delta G_{PB}$

[c] Total nonpolar contribution: $\Delta G_{np} = \Delta E_{vdw} + \Delta G_{SA}$

[d] Glide docking score for initial poses.